The Astrophysical Journal, 817:94 (9pp), 2016 February 1 doi:10.3847/0004-637X/817/2/94

ALFVÉN WAVE HEATING OF THE SOLAR CHROMOSPHERE: 1.5D MODELS

T. D. Arber[1], C. S. Brady[1], and S. Shelyag[2]
[1] Centre for Fusion, Space and Astrophysics University of Warwick, Coventry, CV4 7AL, UK
[2] School of Mathematical Sciences, Monash University, Clayton, 3800, Australia
Received 2015 October 13; accepted 2015 December 16; published 2016 January 25

ABSTRACT

Physical processes that may lead to solar chromospheric heating are analyzed using high-resolution 1.5D non-ideal MHD modeling. We demonstrate that it is possible to heat the chromospheric plasma by direct resistive dissipation of high-frequency Alfvén waves through Pedersen resistivity. However, this is unlikely to be sufficient to balance radiative and conductive losses unless unrealistic field strengths or photospheric velocities are used. The precise heating profile is determined by the input driving spectrum, since in 1.5D there is no possibility of Alfvén wave turbulence. The inclusion of the Hall term does not affect the heating rates. If plasma compressibility is taken into account, shocks are produced through the ponderomotive coupling of Alfvén waves to slow modes and shock heating dominates the resistive dissipation. In 1.5D shock coalescence amplifies the effects of shocks, and for compressible simulations with realistic driver spectra, the heating rate exceeds that required to match radiative and conductive losses. Thus, while the heating rates for these 1.5D simulations are an overestimate, they do show that ponderomotive coupling of Alfvén waves to sound waves is more important in chromospheric heating than Pedersen dissipation through ion–neutral collisions.

Key words: magnetohydrodynamics (MHD) – Sun: chromosphere

1. INTRODUCTION

Alfvén waves have been proposed as an energy delivery mechanism for solar atmospheric processes ranging from heating of the chromosphere (Osterbrock 1961; van Ballegooijen et al. 2011) or corona (Kudoh & Shibata 1999; van Ballegooijen et al. 2011) to the acceleration of the solar wind (De Pontieu 2007). Both observations (De Pontieu 2007) and numerical models (e.g., Shelyag et al. 2012, 2013) show that there is enough Alfvén wave energy generated in the convection zone to heat the chromosphere, but the mechanisms by which this wave energy is thermalized in the chromosphere, if indeed it is, remain unclear. If Alfvén waves are a dominant source of quiet chromospheric heating the observed input flux of $\sim 10^7$ erg cm^{-2} s^{-1} must be converted into a $\sim$0.1 erg cm^{-3} s^{-1} local heating rate to balance the energy loss in the chromosphere. Estimates place the maximum heating rate required as $\sim$0.1 erg cm^{-3} s^{-1} dropping to $\sim 10^{-3}$ erg cm^{-3} s^{-1} in the upper chromosphere (Ulmschneider 1974; Avrett 1981).

The possibility that Alfvén waves may heat the solar atmosphere and drive the solar wind has been studied numerically with many variations. Hollweg (1978, 1981, 1992) and Hollweg et al. (1982) extensively studied the 1.5D problem for circularly polarized Alfvén waves in expanding flux tubes and showed the importance of coupling to slow modes, fast modes and shocks. These papers demonstrated that it was certainly possible for Alfvén waves to heat the solar atmosphere and drive the solar wind. Later work has extended this to white noise spectrum photospheric drivers in both 1.5D (Kudoh & Shibata 1999) and 2.5D (Matsumoto & Suzuki 2012). The main focus of these papers has been on coronal heating and driving the solar wind. Thus, while they contained model atmospheres with chromospheres and transition regions, these were not modeled with very high resolution, nor were detailed heating profiles produced specifically for the chromosphere. Despite this, all papers listed above did show that a heating rate broadly consistent with the requirements of both the chromosphere and corona was possible for photospheric motions with speeds of order $\sim$1 km s^{-1} driving Alfvénic perturbations.

Matsumoto & Suzuki (2014) extended their original analysis (Matsumoto & Suzuki 2012) and improved the diagnostics for shock heating and concluded that shock heating was the dominant heating mechanism in the chromosphere. These simulations did not explicitly include resistivity or assess the sensitivity of these results to the chosen driver spectrum. Nonetheless they present a compelling case for shock heating of the chromosphere originating from a broad spectrum photospheric, Alfvénic driver. The results presented below represent an extension of this line of work, albeit only in one spatial dimension, to assess the importance of explicit resistive dissipation through electron–ion, electron-neutral, and ion–neutral collisions. Also studied is the sensitivity of the results to the chosen driver spectrum and a high-resolution focus on just the chromosphere.

Turbulence has long been proposed as a possible mechanism by which the input driver wave energy could be dissipated (Hollweg 1986). Direct dissipation of driver Alfvén waves through resistive effects is too slow to explain the required heating rate. However, if a turbulent cascade exists which can transfer the driver energy to higher wavenumbers where dissipation does occur there is sufficient wave energy in the chromosphere to balance radiative losses. This theory does however leave unanswered the question of whether a turbulent cascade to dissipation scales does actually exist in the chromosphere. Reduced MHD models have recently concluded that Alfvén waves may drive a turbulent cascade, through reflection off the transition region, which could heat the chromosphere (van Ballegooijen et al. 2011). The implementation of reduced MHD in van Ballegooijen et al. (2011) ignores compressive effects so does not permit coupling of Alfvén waves to slow modes or the formation of shocks.

Studies of the resistive dissipation of Alfvén waves by collisions between ions and neutral atoms, begun with

Piddington (1956), have recently begun to be re-investigated and extended (De Pontieu et al. 2001; Leake et al. 2005; Goodman 2011; Tu & Song 2013). The temperature variation through the chromosphere means that it contains both regions where the hydrogen is near fully ionized and regions where only heavy ions with a low first ionization potential are ionized (Vernazza et al. 1981; Fontenla et al. 1993; Avrett & Loeser 2008). Under low-ionization conditions the ion and neutral gas fluids partly decouple, and energy dissipation due to ion–neutral collisions is orders of magnitude more important than the resistivity resulting from electron–ion Coulomb collisions (Khodachenko et al. 2004; Khomenko & Collados 2012). Previous work in this area has shown efficient heating of both the upper chromosphere (De Pontieu et al. 2001; Leake et al. 2005) and the lower chromosphere (Goodman 2011; Song & Vasylunas 2011; Tu & Song 2013) due to ion–neutral collisions.

Numerical simulations in this area are complicated by the simultaneous requirements to resolve short driver wavelengths and a high Alfvén speed in the upper chromosphere. Tu & Song (2013) also include the Hall term in chromospheric heating models further reducing the timestep in the simulations. The computational effort that is required to simultaneously resolve all of these length and time scales means that 1.5D modeling is often used to model Alfvén wave propagation and heating in the chromosphere (Leake et al. 2005; Tu & Song 2013). These have shown that Alfvén waves with periods much less than 10 s are effectively damped by Pedersen resistivity (De Pontieu et al. 2001; Leake et al. 2005) in the chromosphere, and for incompressible simulations with a Kolmogorov driving spectrum the heating is primarily in the lower chromosphere and sufficient to balance radiative losses there (Tu & Song 2013).

There is therefore compelling observational and theoretical evidence that a significant fraction of the heating requirements of the upper chromosphere, and possibly the quiet corona, could be accounted for through the dissipation of Alfvén wave energy, or MHD waves in general in geometries which make pure Alfvén waves unlikely. This paper extends the earlier works by concentrating specifically on the chromosphere and varying the spectrum of driven Alfvén waves, solving the full compressible MHD equations and including partially ionized plasmas. Section 1 covers the assumptions made, the numerical method and driver spectra used in the simulations. Since much previous work on turbulent heating (van Ballegooijen et al. 2011; Tu & Song 2013) assumed an incompressible plasma incompressible results are presented in Section 3. Full compressible simulations results are presented in Section 4 and conclusions which can be drawn from these 1.5D simulations are in Section 5.

2. MODEL EQUATIONS

This paper presents the results of numerical simulations performed using the Hall-MHD code LARE (Arber et al. 2001). This code solves the ideal MHD equations explicitly using the Lagrangian remap approach and includes the resistive and Hall terms using explicit subcycling. The complete set of MHD equations relevant in this case are

$$\frac{D\rho}{Dt} = -\rho\nabla.\,\boldsymbol{v} \tag{1}$$

$$\rho\frac{D\boldsymbol{v}}{Dt} = \boldsymbol{j}\times\boldsymbol{B} + \rho\boldsymbol{g} - \nabla P + \boldsymbol{F}_{\rm shock} \tag{2}$$

$$\frac{\partial\boldsymbol{B}}{\partial t} = -\nabla\times\boldsymbol{E} \tag{3}$$

$$\frac{D\epsilon}{Dt} = -\frac{P}{\rho}\nabla.\,\boldsymbol{v} + \frac{H_{\rm visc}}{\rho} + \frac{H_{\rm Ohmic}}{\rho} \tag{4}$$

$$\boldsymbol{j} = \frac{1}{\mu_0}\nabla\times\boldsymbol{B} \tag{5}$$

$$\boldsymbol{E} = -\boldsymbol{v}\times\boldsymbol{B} + \eta\boldsymbol{j}_{\parallel} + \eta_p\boldsymbol{j}_{\perp} + \frac{1}{en_{\rm e}}\boldsymbol{j}\times\boldsymbol{B} \tag{6}$$

where ρ is the mass density, P is the ideal gas pressure, $\boldsymbol{B}$ is the magnetic field, $\boldsymbol{v}$ is the fluid velocity, $\boldsymbol{E}$ is the electric field, ϵ is the specific internal energy density, n_e is the electron number density, e is the proton charge, and $(\boldsymbol{j}_{\parallel},\boldsymbol{j}_{\perp})$ are the current densities parallel/perpendicular to the local magnetic field. These equations are in written in Lagrangian form where

$$\frac{D}{Dt} = \frac{\partial}{\partial t} + \boldsymbol{v}.\,\nabla$$

is the usual advective derivative. Shock viscosity is added to the momentum equation through $\boldsymbol{F}_{\rm shock}$ which has a functional form which vanishes for smooth flows in the limit of increasing resolution but remains finite at discontinuities. Thus the shock jump conditions are satisfied through an appropriate shock viscosity as in Caramana et al. (1998) and Arber et al. (2001). In this formulation shock heating can therefore be monitored though viscous heating. Hence viscous heating and shock heating are used as synonyms throughout the rest of this paper.

Missing from Equation (4) are thermal conduction, radiative losses and all non-local radiation transport. To prevent the atmosphere heating up without bounds due to the viscous dissipation of shocks ($H_{\rm visc}$) and Ohmic heating ($H_{\rm Ohmic}$), both $H_{\rm visc}$ and $H_{\rm Ohmic}$ are calculated in simulations as a diagnostic but only $H_{\rm visc}$ is added to the energy update. If $H_{\rm visc} = 0$, as in incompressible simulations, ignoring $H_{\rm Ohmic}$ assumes that the background atmosphere is for a slowly varying chromosphere where heating terms are approximately balanced by losses. Shock heating must be included in compressible simulations otherwise the shocks themselves are not treated correctly. This leads to a heating of the chromosphere. Despite this the ionization state is held fixed at its initial equilibrium value. Since shock heating, which is only weakly sensitive to the ionization state, dominates in these simulations this will not change the heating rates by more than a factor ∼2.

The resistive MHD Ohm's law for a fully ionized plasma is $\boldsymbol{E} = -\boldsymbol{v}\times\boldsymbol{B} + \eta_{\parallel}\boldsymbol{j}_{\parallel} + \eta_{\perp}\boldsymbol{j}_{\perp}$ (Braginskii 1965) where

$$\eta_{\perp} = \frac{m_{\rm e}\nu_{\rm ei}}{n_{\rm e}e^2}$$

is the classical electron–ion resistivity resulting from Coulomb scattering and $\nu_{\rm ei} = 3.7\times n_{\rm i}\log(\Lambda)/T^{3/2}$ is the electron–ion collision frequency for ion number density $n_{\rm i}$ and Coulomb logarithm $\log(\Lambda)$. $\eta_{\parallel} = 0.51\eta_{\perp}$ and the resistivity is anisotropic. Normally within solar and space physics, where the Lundquist number is high, this is simplified to $\boldsymbol{E} = -\boldsymbol{v}\times\boldsymbol{B} + \eta_{\perp}\boldsymbol{j}$ with an isotropic resistivity. This approximations is adopted in this paper so Ohmic dissipation resulting from parallel currents is likely to be over estimated by a factor ≃2. In the 1.5D

simulations in this paper there can be no current along the background magnetic field so the leading order Ohmic dissipation from electron–ion collisions is for perpendicular currents.

In Equation (6), η is the classical resistivity resulting from electron collisions with ions and neutrals and η_p the Pedersen resistivity (Cowling 1957; Leake et al. 2005). Explicitly the resistivities used in this paper are

$$\eta = \frac{m_e \nu_e}{n_e e^2}$$

where ν_e is the electron collision frequency including collisions with ion and neutrals. The Pedersen resistivity is then given by

$$\eta_p = \eta + \frac{\xi_n^2 B^2}{(1-\xi_n)} \frac{1}{\rho \nu_{in}} \quad (7)$$

where $\xi_n = m_i n_n / \rho$ is the neutral fraction with n_n the number density of neutrals. The ion–neutral collision frequency is given by

$$\nu_{in} = n_n \sqrt{\frac{16 k_B T}{\pi m_i}} \Sigma_{in}$$

here $\Sigma_{in} = 5 \times 10^{-19}\,\mathrm{m}^2$ is the cross-section for ion–neutral collisions for hydrogen from Osterbrock (1961) and De Pontieu & Haerendel (1998). For an effective ion mass of 1.2 proton masses $\nu_{en} \simeq 5\nu_{in}$. The pressure gradient term $-\nabla P_e$ is ignored in Equation (6) as this can only generate a parallel electric field in 1.5D simulations which have no effect on the dynamic equations.

In the above descriptions of resistivities we have adopted the nomenclature used in (Leake et al. 2014). Following Leake et al. (2014) we also use Cowling resistivity (η_c), defined as $\eta_c = \eta_p - \eta$, to refer to that component of perpendicular resistivity which arises purely due to ion–neutral collisions. It is important to note that the Pedersen resistivity is only the inverse of the Pedersen conductivity, more commonly used in ionospheric physics, if the Hall term is zero.

The inclusion of neutrals in a single-fluid model, as described above, is valid in the same limit as resistive MHD, i.e., timescales larger than the gyro-period, collision times and the plasma period and length-scales larger than the ion gyroradius and collisional mean-free-path. The only additional constraint, compared to single fluid MHD, is therefore that Equations (1)–(6) are only valid for times larger than the ion–neutral collision time. In the chromosphere this can be as low as a millisecond so the model is valid up to frequencies of $\simeq 10^3$ Hz.

In all simulations the x axis is ignorable, the y axis extends vertically up from the solar surface starting at the $\tau = 1$ optically thick surface, and the z axis is also ignorable, while velocities in the z direction are allowed and associated with Alfvénic perturbations. The upper boundary condition is kept open by the use of both Riemann characteristic open boundaries and a damping region where the simulation velocity is smoothly reduced as it approaches the boundary. The measured reflection of the upper boundary is less than 0.01%. In some sections LARE is converted into a 1.5D incompressible code by setting the forces parallel to the y axis to zero. This sets $v_y = 0$, which in 1.5D is equivalent to the incompressible condition $\nabla \cdot \boldsymbol{v} = 0$.

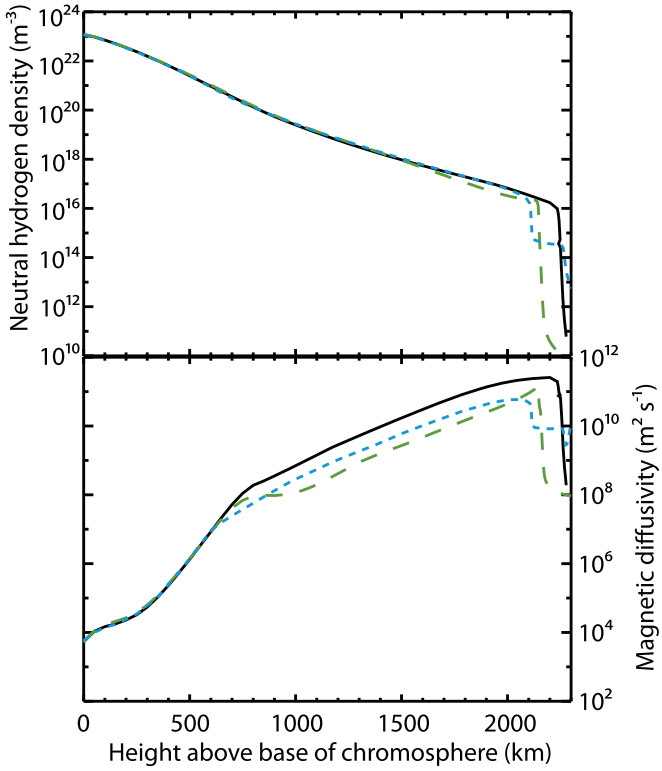

Figure 1. (a) Calculated neutral hydrogen density as a function of height above the base of the photosphere for different atmospheric models. (b) Magnetic diffusivity (η_p/μ_0) as a function of height above the base of the photosphere for different atmospheric models. Black line corresponds to FAL A (Fontenla et al. 1993), green long dashed line—to Avrett and Loeser C7 (Avrett & Loeser 2008), and blue short dashed line—to VAL C (Vernazza et al. 1981) model.

For the simulations presented in this paper, a model atmosphere based on the semi-empirical C7 model of Avrett & Loeser (2008) is used for the initial temperature profile. This is then integrated iteratively to provide a density profile which is in hydrostatic equilibrium. On each iteration the ionization state of the plasma is calculated under the assumption of local thermal equilibrium using a two level Athay potential model (Leake & Arber 2006) until a converged density is obtained. The background magnetic field B_y is assumed to be a uniform vertical 50 G. This is chosen as a representative value averaged along an inter-granular field line.

Figure 1 plots neutral density and Pedersen diffusivity for the Avrett and Loeser C7 atmosphere model in this paper. For comparison, Figure 1 also shows the same plots for the two other atmospheric models: the VAL III C model of Vernazza et al. (1981) and the FAL A model of Fontenla et al. (1993). It is found that the density of neutral hydrogen predicted by the Athay potential model and the associated Pedersen resistivity are similar in all cases although the FAL A model does predict 5 times greater Pedersen resistivity in the upper chromosphere. Figure 2 shows the temperature and Alfvén speed profiles for the Avrett and Loeser C7 atmosphere model with an imposed background 50 G field.

2.1. Boundary Driving and Poynting Flux

Alfvén waves are introduced into the domain by driving the bottom boundary of the simulation. The velocity field is prescribed by Equation (8) to give a kinetic energy spectrum

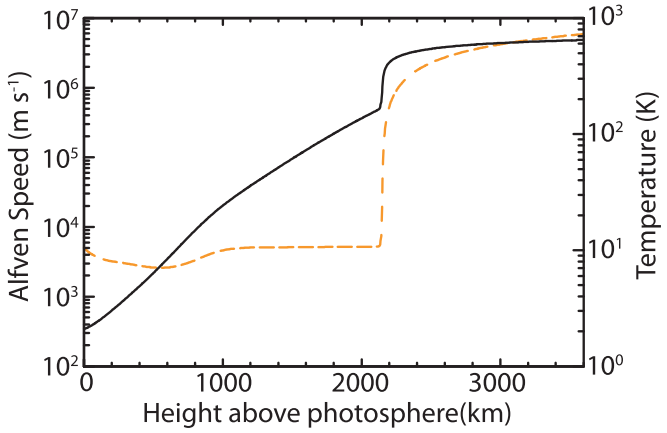

Figure 2. Temperature profile (dashed line) and Alfvén speed (solid line) for a 50 G background field and the Avrett and Loeser C7 atmosphere model.

consisting of two regions—the low frequency region, where the power in a mode increases with frequency, and a Kolmogorov region at higher frequency, where power drops as $k^{-5/3}$:

$$v_z = A\left(\sum_{i=0}^{N_1}\omega_i^{\frac{5}{6}}\sin(\omega_i t+\phi_i)+\sum_{j=0}^{N_2}\omega_j^{-\frac{5}{6}}\sin(\omega_j t+\phi_j)\right) \quad (8)$$

ω_i is the frequency of mode i in the low frequency region and in this paper runs from 0.001 to 0.01 Hz, ω_j is the frequency of mode j in the high frequency region and in this paper runs from 0.01 Hz to an arbitrary upper cutoff frequency which ranges between 0.1 and 10 Hz. ω_i and ω_j are both linearly spaced in frequency. v_z is the velocity component out of the plane of the simulation which is associated with an Alfvén wave. N is the number of harmonics used to produce the driver spectrum and is a large enough number to ensure that the spectrum is reproduced smoothly and that further increase in N does not lead to changes in the heating rate greater than 1%. $N_1 + N_2$ is set to 10,000 for simulations with a 10 Hz upper cutoff frequency, 1000 for simulations with a 1 Hz upper cutoff frequency and 100 for simulations with a 0.1 Hz upper cutoff frequency. Convergence testing using 100,000 driver elements for a simulation with a 10 Hz upper cutoff shows that the result is not sensitive to this parameter so long as the total Poynting flux through the photospheric lower boundary is kept constant. $\phi_{i,j}$ is the phase for spectral component i or j and is selected randomly for each mode.

The amplitude A is selected to give a total energy flux at the bottom boundary of 10^7 erg cm^{-2} s^{-1}. This corresponds to a velocity field with an rms value of 415 m s^{-1} at the $\tau = 1$ optically thick photospheric surface, comparable with observations of photospheric transverse velocities (see, for example, Chae 2001 or Nindos & Zhang 2002). The spectra of the used drivers, for differing cutoff frequencies, are show in Figure 3. This form of the driver is based on that used by Tu & Song (2013), although they specified a net average Poynting flux of 2×10^7 erg cm^{-2} s^{-1}. There is no observational evidence for such a driver spectrum. Instead this has been chosen so that the rms velocity matches observations along with the total Poynting flux, which constrains the magnetic field once photospheric densities and velocities are defined. Equation (8) therefore has observationally constrained average velocity and

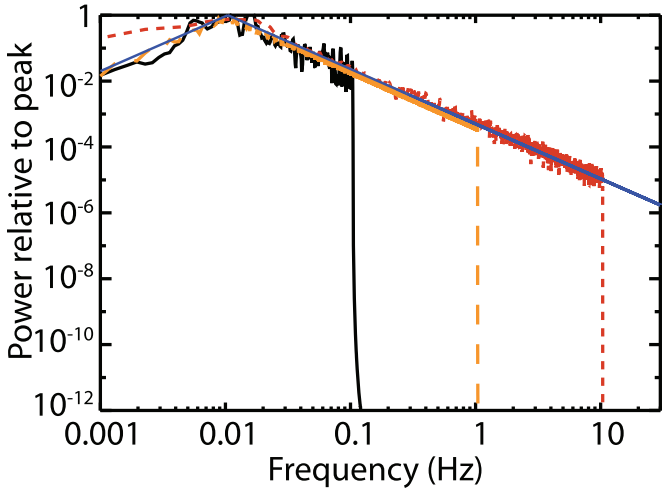

Figure 3. Driver spectra with different upper cutoff frequencies. 10 Hz (Red short dashed line), 1 Hz (Orange long dashed line) and 0.1 Hz (Black solid line) upper cutoff are shown with overplotted blue solid lines showing the envelope from the two terms in Equation (8).

integrated flux. There is no direct evidence for high frequency Alfvén waves thus the choice of a Kolmogorov spectrum is motivated purely by the observation that the photospheric motion is turbulent and hence some scale-free power-law dependence is expected. The results are insensitive to the choice of spectrum in the rising part of the spectrum, which could have been chosen to be flat, other than its effect on the amplitude limiting to specify the net Poynting flux.

The net Poynting flux from the specified velocity driving on the photosphere needs to be calculated from the simulations. In the single fluid MHD model this can be rewritten as

$$\boldsymbol{S}(\boldsymbol{r}, t) = \mu_0^{-1}\boldsymbol{B}(\boldsymbol{r}, t) \times (\boldsymbol{v}(\boldsymbol{r}, t) \times \boldsymbol{B}(\boldsymbol{r}, t)) \quad (9)$$

where $\boldsymbol{v}$ is the fluid centre of mass velocity, and $\boldsymbol{B}$ is the magnetic field. The commonly used approximation

$$S = \langle v_z^2\rangle c_{\rm A}\rho \quad (10)$$

where v_z is the velocity amplitude perpendicular to the magnetic field and $c_{\rm A}$ is the local Alfvén speed, fails for the photospheric driver as this is a linear approximation for waves propagating only in one direction. At the photosphere, where there are reflected waves from the transition region, this approximation is not valid. This is demonstrated in Figure 4, where the time-integrated Poynting vector calculated using both Equations (9) and (10) through the lower boundary of a simulation of the solar chromosphere with no dissipation mechanisms present are shown. These agree up until the first driven Alfvén waves from the driver have returned after partial reflection from the transition regions, around 160 s, at which point they diverge. Equation (10) overestimates the total Poynting flux through the boundary by a factor of up to 2. This means that estimates of Poynting flux obtained using Equation (10), whether from simulation or observation, are almost certain to be overestimated. In this paper the Poynting flux is always calculated using the form in Equation (9).

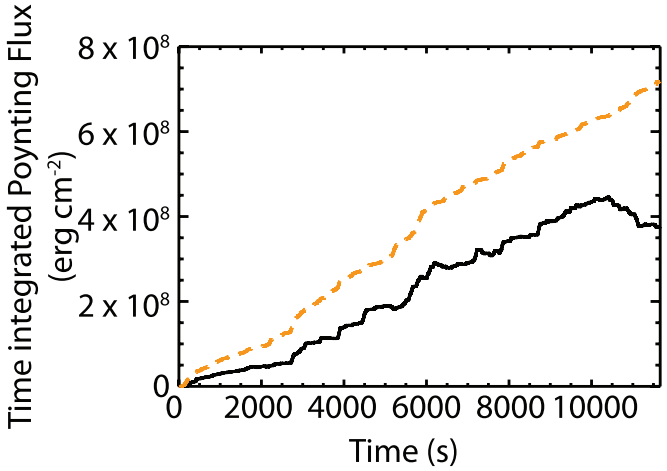

Figure 4. Time-integrated Poynting flux through the lower boundary of a simulation of Alfvén waves propagating into the solar chromospheric cavity. The black solid line is calculated using Equation (9), orange dashed line using Equation (10).

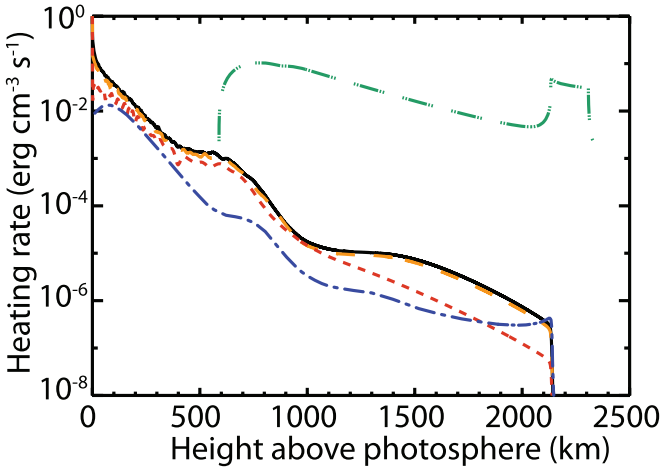

Figure 5. Heating rate as a function of height for incompressible simulations of Alfvén waves driven into a C7 model atmosphere. The upper cutoff frequency is 0.1 Hz in the simulation shown by the red short dashed line, 1 Hz by the orange long dashed line, and 10 Hz by the black solid line. The blue line is the analytic estimate from Equation (16). The green dot–dot–dash line is the estimated heating requirement for the quite chromosphere taken from Avrett (1981).

3. INCOMPRESSIBLE MODEL

Using the 1.5D setup as previously described and assuming that the plasma is incompressible ($\nabla \cdot \boldsymbol{v} = 0$, $v_y = \text{const}$), the MHD Equations (2)–(6) simplify to

$$\rho \frac{\partial v_z}{\partial t} = \frac{1}{\mu_0} B_y \frac{\partial B_z}{\partial y}, \tag{11}$$

$$\frac{\partial B_z}{\partial t} = B_y \frac{\partial v_z}{\partial y}. \tag{12}$$

Normalizing to the constant vertical field and the local Alfvén speed such that $B_z = B_y b$ and $v_z = c_A v'$ it is possible to rewrite these equations in terms of the Elsässer variables $z^{\pm} = v \pm b$, where z^- and z^+ correspond to upwards and downwards propagating Alfvén waves respectively. After dropping the primes for normalized variable Equations ((11)–(12)) are

$$\frac{\partial z^{\pm}}{\partial t} \mp c_A \frac{\partial z^{\pm}}{\partial y} = \pm \frac{(z^+ + z^-)}{2} \frac{\partial c_A}{\partial y}. \tag{13}$$

There is no nonlinear coupling between upward propagating and downward propagating waves which would lead to a cascade, i.e., no nonlinear interaction between z^+ and z^-. Alfvén turbulence is suppressed in 1.5D by the assumption of incompressibility. Thus energy introduced by the driver in a given frequency will stay in that frequency until it is either dissipated or leaves the computational domain. LARE is converted to a 1.5D incompressible code as described in Section 1 and used to simulate an Alfvén wave spectrum given by Equation (8) propagating into the Avrett & Loeser C7 model atmosphere. 4096 grid points are used in the y direction, and a length of 6000 km above the visible solar surface is simulated for all results, even those for which results are only plotted for the chromosphere. At heights above 4500 km the velocity damping region is applied. Convergence is tested with a simulation of 8192 grid points, resulting in a change in the solution of $<1\%$ as measured by the heating rate.

Simulating an Alfvén wave spectrum given by Equation (8) with a high frequency cutoff of 0.1 Hz, 1 Hz, or 10 Hz propagating up into the C7 atmosphere (Figure 5), it is found that heating is highest in the photosphere with a local maximum at the temperature minimum. This is comparable to the results in Goodman (2011) and Tu & Song (2013) who used a similar model to that presented here. Since resistive dissipation is more effective for shorter wavelengths and there is no turbulent cascade, the choice of upper cutoff frequency for the driver would be expected to affect the efficiency of the dissipation. This is observed in Figure 5 where greater heating at all heights is observed if a higher upper cutoff frequency in the driver spectrum is chosen. The simulations produce heating rates comparable to those in Tu & Song (2013), with or without the Hall term included in Ohm's law. The Hall term is found to have negligible effect ($<0.01\%$) on the heating rate in all simulations. Note that the three lines in Figure 5 are from driver spectra where the amplitudes have been changed so that the net Poynting flux is the same in all three cases. For the 10 Hz cutoff the total heating rate in the chromosphere is only of the order of 10^3 erg cm^{-2} s^{-1}. The majority of the input energy in these simulations goes into increasing the energy stored in long wavelength Alfvén waves in the chromosphere and not into heating. A fraction of the total input power does leak into the corona, see later, but the continual buildup of Alfvén wave energy at long wavelength throughout the simulations, while correct for the incompressible simulations, is unphysical and can only be corrected by the inclusion of compressibility.

As with Goodman (2011) and Tu & Song (2013) it is found that heating in the photosphere and low chromosphere is dominated by dissipation due to classical resistivity (Figure 6) while heating in the upper chromosphere is mainly due to Cowling resistivity. The largest heating rates occur in the parts of the simulation that are dominated by electron–ion and electron-neutral resistivity.

The qualitative features of Figure 5 can be reproduced with a simple analytic approach. This assumes that the heating is from a single pass of Alfvén waves and all wavelengths are less than the density scale height. If only Alfvén waves are present then the Alfvén wave energy $U(y) = \rho(y) v_z^2(y)$ is determined by

$$\frac{\partial U}{\partial t} + \frac{\partial S}{\partial y} = -\eta j^2 \tag{14}$$

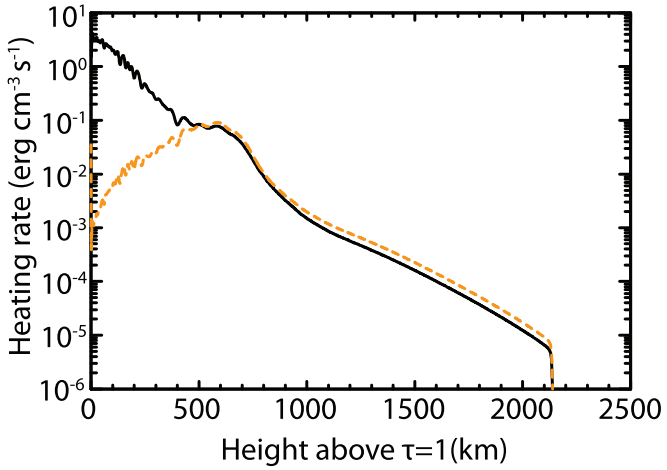

Figure 6. Heating rate as a function of height for the full incompressible simulation including Pedersen resistivity η_p, Equation (7) (black solid line) or Cowling resistivity only, $\eta_c = \eta_p - \eta$ (orange dashed line) with a 0.1 Hz cutoff in the driver spectrum.

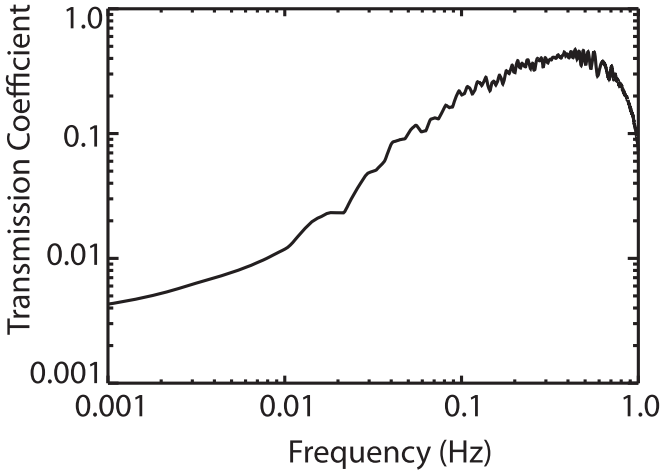

Figure 7. Spectral energy transmission coefficient of the photospheric cavity from incompressible simulations.

with S given by Equation (10) and η the total resistivity. Since $S = c_A U$ in steady state, this can be solved to give

$$U(y) = U(0)\frac{c_A(0)}{c_A(y)}\exp\left[-\omega^2\int_0^y \frac{\eta(y')}{\mu_0 c_A(y')^3}\,dy'\right]. \quad (15)$$

In this linearized WKB approach with only upward propagating Alfvén waves the local heating rate $h(y, \omega)$ is given by

$$h(y, \omega) = U(0)\frac{\eta(y)c_A(0)}{\mu_0 c_A(y)^3}\exp(-\omega^2 F(y)), \quad (16)$$

where

$$F(y) = \int_0^y \frac{\eta(y')}{\mu_0 c_A(y')^3}\,dy'. \quad (17)$$

Integrating over ω then gives the local heating rate for an incompressible chromosphere under the assumption that all the heating is from a single upward propagating pass through the chromosphere and transition region, i.e., ignoring reflection. This analytic heating rate is plotted in Figure 5. The discrepancy between the simplified analytic model and full simulations are due to the WKB approximation and the absence of reflected waves in the analysis leading to Equation (16). Also plotted on Figure 5 is an estimate of the required volumetric heating rate as a function of height taken from (Avrett 1981). This heating rate is not well defined below the temperature minimum.

For the incompressible simulations there is no coupling between modes in 1.5D. As a result it is easy to estimate the effective transmission coefficient of the transition region as a function of frequency without the complication which would arise from mode coupling in a nonlinear simulation. The transmission coefficient is calculated as the ratio of the Poynting flux, as a function of frequency, just above the transition region to the Poynting flux at the base of the simulation domain. This is then smoothed with a boxcar moving average of 0.005 Hz width and plotted in Figure 7. Transmission ranges between 40% at 0.5 Hz to 0.32% at 0.001 Hz. Only higher frequencies have appreciable transmission coefficients as the shorter wavelengths "see" a density ramp rather than a discontinuity at the transition region. For frequencies above 0.5 Hz the measured transmission drops due to these frequencies been damped by Pedersen resistivity before they reach the transition region.

The overall energy budget from incompressible simulations is therefore that high frequency, i.e., greater than 0.1 Hz, Alfvén waves can both heat the upper chromosphere and leak into the corona. The majority of the chromospheric heating in incompressible simulations come from these high-frequency waves. For the chosen power law spectrum with rms amplitude $\sim$400 m s^{-1} at the photosphere the typical heating rate above 1000 km is of the order of 10^{-6}–10^{-5} erg cm^{-3} s^{-1} for a 50 G vertical field. The peak chromospheric heating required to balance radiative and conductive losses are $\sim$0.1 erg cm^{-3} s^{-1} with rates of $\sim 10^{-3}$ erg cm^{-3} s^{-1} needed in the upper chromosphere (Ulmschneider 1974). Higher heating rates could be achieved with the Kolmogorov driver used here by choosing a stronger background field strength or alternatively a higher rms velocity driver could be used. Either of these would however increase the Poynting flux in the observed low-frequency part of the spectrum and thus contradict observations. Another possibility is that distribution of Alfvén waves deviates significantly from a $-5/3$ power law and has more energy at higher frequencies. This would require orders of magnitudes more energy in the high-frequencies contradicting our assumption of a turbulent photospheric driver with a power-law spectra and is not studied further here.

4. COMPRESSIBLE MODEL

The incompressible model in 1.5D cannot be turbulent and there is no cascade of energy to smaller scales. The heating rate from Pedersen resistivity can be made to match the chromospheric heating requirements by ensuring sufficient energy is input into the base of the simulation in frequencies which are damped by ion–neutral collisions. The heating rates as a function of height are therefore entirely dependent on the user-specified input spectrum which for these frequencies is poorly constrained by observations. Work by Hollweg et al. (1982) and others have also shown the importance of ponderomotive coupling of Alfvén waves to slow and fast modes in a compressive medium. In this section we repeat the simulations

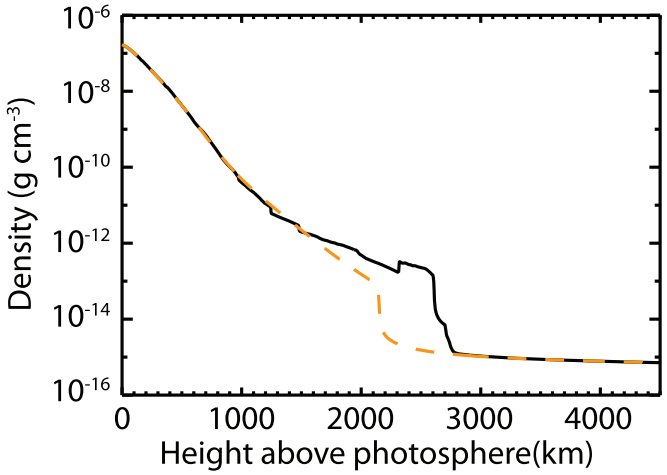

Figure 8. Density at the start of the simulation (orange dashed line) and at 20 Alfvén transit times of the photospheric cavity (black line) from compressible simulations.

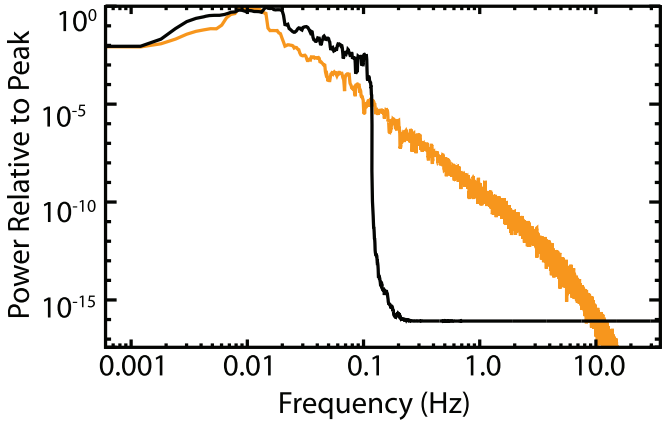

Figure 9. Spectral energy in driver at the base of the simulation domain (black line) and in the upper chromosphere (orange line) from compressible simulations. Both lines are smoothed with a boxcar moving average of width 0.05 Hz.

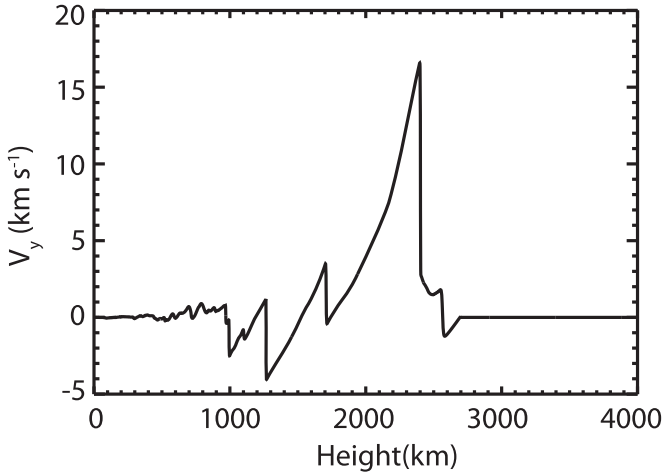

Figure 10. Velocity component parallel to the background magnetic field with height, showing the formation of discontinuities from compressible simulations.

of Section 3 for the full set of compressible MHD equations. As before the heating due to Pedersen resistivity is calculated but not added into the simulation thermal energy. This approach is not possible for the shock heating which is allowed in compressible simulation, as this is required to ensure the correct shock jump conditions. An inevitable consequence of this is that the model atmosphere heats up due to shock dissipation. The Pedersen resistivity is however kept at the same profile as derived from the initial conditions. In the absence of conductive and radiative losses the shock heating would ionize the chromosphere and turn-off Cowling resistivity, i.e., that part of the Pedersen resistivity due to ion–neutral collisions. This lack of self-consistency is shown below to not be significant as the dominant heating is through shock dissipation not resistivity.

A limitation of the 1.5D model used here is that the net ponderomotive force from a persistent photospheric driver lifts the transition region and changes the atmospheric density structure. This is shown in Figure 8. In a compressible simulation energy cascades to shorter scale-lengths are now permitted. This can clearly be seen in Figure 9, where the spectral energy in Alfvén waves from a driver introducing wave energy between 0.001 and 0.1 Hz (black line) is compared to the energy present in the upper chromosphere (2000 km above the photospheric surface). Power at frequencies above the driver cutoff are clearly present in the upper chromosphere. This is not a purely Alfvénic cascade as it shows the characteristic -2 spectral power of a shock dominated system, but it does provide a mechanism by which shorter length scales can be created self-consistently within the simulation. As a check of the simulations for consistence against observations we note that the velocity field 2000 km above the photosphere in these simulations is 23 ± 2 km s^{-1}. Transverse velocities observed for spicules by De Pontieu et al. (2007) were 20 ± 5 km s^{-1}.

Figure 10 shows that slow mode shocks are produced in the simulations. Since the entropy jump across the shock can heat the plasma, care must be taken to correctly reproduce this shock heating. In order to ensure that shocks in the simulations satisfy the entropy condition in the shock jump relations, LARE uses the artificial viscosity formulation of Caramana et al. (1998) and Arber et al. (2001), which both viscously change the velocity and deposits the associated viscous heating. In the limit of infinite resolution this viscosity goes to zero in smooth regions of the solution and satisfies the shock jump conditions at discontinuities. However, at finite resolution viscosity is erroneously applied to parts of the solution which are steep on the scale of the grid, but are not true discontinuities. This means that careful convergence testing of the results of the simulations is required to confirm that the heating is due to shocks and not due to numerical error. This is shown in Figure 11 where it is shown that shock heating is more important in the upper chromosphere than resistive heating, and also that the shock heating rate is converged in these simulations to within 10% in the chromosphere. While shock heating rates in the photosphere are not converged, they are clearly lower than the well-converged resistive heating rate at those heights. The light red dash dot line on Figure 11 shows the heating rate from the incompressible simulations. It can be seen that the overall resistive heating rate is similar in both compressible and incompressible simulations, but that additional resistive heating in the upper chromosphere is observed in the compressible simulations. Despite this, it is still 4 orders of magnitude lower than the shock heating rate.

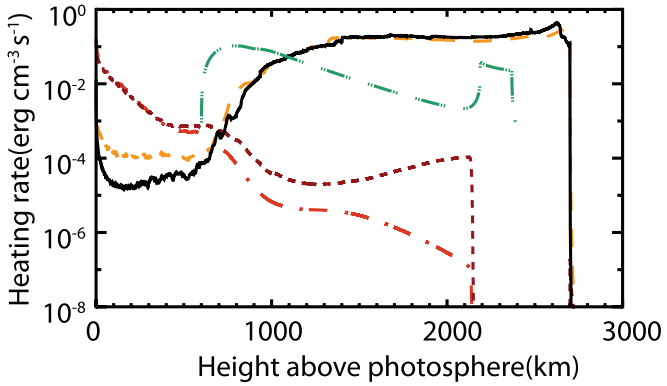

Figure 11. Heating rate with height in compressible simulations of two different resolutions. The orange dashed line is shock heating in a simulation of 8192 grid cells with a driver cutoff frequency of 1 Hz, the black solid line shock heating in a simulation of 16,872 grid cells with the same cutoff frequency. The dark red short dashed line is the resistive heating from the 16,872 cell compressible simulation, and the light red dash–dot line is from an equivalent incompressible simulation. The green dot–dot–dash line is the estimated heating requirement for the quite chromosphere taken from Avrett (1981).

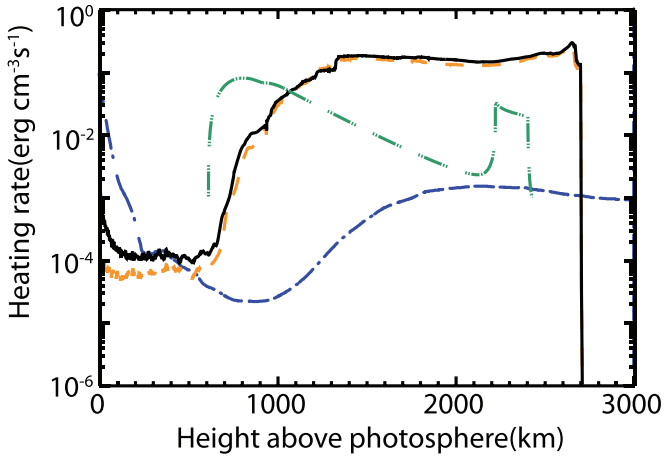

Figure 12. Heating rate with height in compressible simulations with three driver upper cutoff frequencies. Black solid line has upper cutoff frequency of 0.1 Hz, orange dashed line of 1 Hz and blue line 0.01 Hz. The green dot–dot–dash line is the estimated heating requirement for the quite chromosphere taken from Avrett (1981) based on observations.

Figure 12 shows that shock heating in the compressible simulations is the same for both cutoff frequencies above 0.1 Hz. No results are shown for a cutoff of 10 Hz as these are the same as those for 1 Hz. The shock heating rate is higher than the heating rate needed to balance conduction and radiation in the chromosphere for a realistic driver amplitude. This may explained by artificial effects of these 1.5D simulations. In particular, the missing vertical structure of the magnetic field and the artificial enhancement of shock strength due to shock coalescence—only possible in 1.5D. It is therefore possible to limit the heating due to Pedersen resistivity by imposing a cutoff on photospheric driver frequencies of 0.1 Hz while maintaining the same level of shock heating. The extent to which this may be true in a realistic chromosphere cannot be addressed in 1.5D models and must be tested in 2D and 3D. For a driver cutoff frequency of 0.01 Hz the shock heating is reduced by three orders of magnitude.

5. CONCLUSIONS

The simulations presented in this paper show that it may be possible to heat the solar chromosphere by dissipating Alfvén wave energy. If energy is present in high enough frequency modes then resistive heating from Pedersen resistivity is sufficient to heat the solar chromosphere directly. The presence of such high frequency modes is not currently observable. However, if compressive effects are included then shock heating is capable of heating the chromosphere for a broad range of driver spectrum in a 1.5D model. In compressible simulations shock heating dominates over resistive dissipation in the upper chromosphere even for driver spectra with high frequency components. A problem with all 1.5D models is that shocks can coalesce and as a result the shock heating reported here is certainly an over-estimate. Also absent from the current model is the flux expansion expected in chromospheric flux tubes. In addition, the possibility that the Alfvén turbulent cascade, which requires at least two spatial dimensions and would be fastest in 3D, may increase the relative importance of resistive dissipation by increasing the rate at which long wavelength Alfvénic energy cascades to the resistive dissipation scale. Despite these omissions from the current 1.5D modeling there are still a number of important conclusions which can be drawn and questions asked to guide future 2D and 3D work.

1. Evidence from over the last 30 years, e.g., references from Hollweg (1981) onwards, have all shown that a low-frequency photospheric driver can excite Alfvén waves which are of sufficient energy to heat the chromosphere through shock heating. The slow modes are generated in the chromosphere via ponderomotive driving. The present study has focused on the chromosphere in more detail, and higher resolution, than previous studies, included Pedersen resistivity and confirmed this potential chromospheric heating mechanism.
2. While the incompressible results from Tu & Song (2013) are confirmed the observed heating as a function of height is entirely a function of the user specified driver since no energy cascade is present. Furthermore this is not changed by the inclusion of the Hall term. Most importantly, the results presented here show that compressible effects dominate the heating by orders of magnitude over Pedersen dissipation in the upper chromosphere.
3. A turbulent cascade leading to heating (Hollweg 1986; van Ballegooijen et al. 2011) is a possible heating mechanism where Alfvén wave energy can be thermalized. However, compressible MHD effects must be included to check if in multi-dimensions the dominant energy loss from a low-frequency driver is through an Alfvén cascade or through coupling to slow modes. The present 1.5D study suggests that coupling to slow modes, which subsequently shock and heat the chromosphere, is the dominant heating mechanism.

In 2D and 3D the Alfvénic turbulent cascade to short scales, and hence dissipation, may be terminated at the dissipation scale of Pedersen resistivity. Alternatively, Alfvénic wave energy may not reach these scales due to energy loss to slow modes via ponderomotive coupling, through mode coupling at the $\beta = 1$ surface or geometric coupling through flux tube

expansion. While only 1.5D, the current study strongly suggests ponderomotive coupling as the dominant mechanism by which Alfvén waves loose energy in the chromosphere. A final possibility is that energy leaks through the transition region (Figure 9) faster than it cascades to the dissipation scale. Only full simulations in 2D and 3D will be able to determine which of these effects is most important.

This work was supported by STFC grant ST/L000733/1 and results were obtained using the DiRAC HPC Facility (www.dirac.ac.uk). This equipment was funded by BIS National E-infrastructure capital grant ST/K00042X/1, STFC capital grants ST/H008519/1 and ST/K00087X/1. Dr. Shelyag is the recipient of an Australian Research Council's Future Fellowship (project number FT120100057). The authors are grateful for the financial support provided by Monash-Warwick Alliance Seed Fund.

REFERENCES

Arber, T. D., Longbottom, A. W., Gerrard, C. L., & Milne, A. M. 2001, JCoPh, 171, 151
Avrett, E. H. 1981, in Proc. Advanced Study Institute, Solar Phenomena in Stars and Stellar Systems, ed. R. M. Donate, & A. K. Dupree (Dordrecht: Reidel), 173
Avrett, E. H., & Loeser, R. 2008, ApJS, 175, 229
Braginskii, S. I. 1965, Transport Processes in a Plasma, Reviews of Plasma physics, Vol. 1 (New York, NY: Consultants Bureau)
Caramana, E. J., Shashkov, M. J., & Whalen, P. P. 1998, JCoPh, 144, 70
Chae, J. 2001, ApJL, 560, L95
Cowling 1957, MagnetoHydroDynamics (New York: Interscience)
De Pontieu, B., & Haerendel, G. 1998, A&A, 338, 729
De Pontieu, B., Martens, P. C. H., & Hudson, H. S. 2001, ApJ, 558, 859
De Pontieu, B. D., McIntosh, S. W., Carlsson, M., et al. 2007, Sci, 318, 1574
Fontenla, J. M., Avrett, E. H., & Loeser, R. 1993, ApJ, 406, 319
Goodman, M. L. 2011, ApJ, 735, 45
Hollweg, J. 1978, SoPh, 56, 305
Hollweg, J. 1981, SoPh, 70, 25
Hollweg, J. 1986, JGR, 91, 4111
Hollweg, J. 1992, ApJ, 389, 731
Hollweg, J., Jackson, S., & Gallaway, D. 1982, SoPh, 75, 35
Khodachenko, M. L., Arber, T. D., Rucker, H. O., & Hanslmeier, A. 2004, A&A, 422, 1073
Khomenko, E., & Collados, M. 2012, ApJ, 747, 87
Kudoh, T., & Shibata, K. 1999, ApJ, 512, 493
Leake, J. E., & Arber, T. D. 2006, A&A, 450, 805
Leake, J. E., Arber, T. D., & Khodachenko, M. L. 2005, A&A, 442, 1091
Leake, J. E., DeVore, C. R., Thayer, J. P., et al. 2014, SSRv, 184, 107
Matsumoto, T., & Suzuki, T. K. 2012, ApJ, 749, 8
Matsumoto, T., & Suzuki, T. K. 2014, MNRAS, 440, 971
Nindos, A., & Zhang, H. 2002, ApJL, 573, L133
Osterbrock, D. 1961, ApJ, 134, 347
Piddington, J. 1956, MNRAS, 116, 314
Shelyag, S., Cally, P. S., Reid, A., & Mathioudakis, M. 2013, ApJL, 776, L4
Shelyag, S., Mathioudakis, M., & Keenan, F. P. 2012, ApJL, 753, L22
Song, P., & Vasylunas, V. M. 2011, JGR, 116, A09104
Tu, J., & Song, P. 2013, ApJ, 777, 53
Ulmschneider, P. 1974, SoPh, 39, 327
van Ballegooijen, A. A., Asgari-Targhi, M., Cranmer, S. R., & DeLuca, E. E. 2011, ApJ, 736, 3
Vernazza, J. E., Avrett, E. H., & Loeser, R. 1981, ApJS, 45, 635